

Magnetic excitations in La-based cuprate superconductors: slave-boson mean-field analysis of the two-dimensional t - J model

Hiroyuki Yamase

*Max-Planck-Institute for Solid State Research,
Heisenbergstrasse 1, D-70569 Stuttgart, Germany*

(Dated: October 11, 2018)

Abstract

Motivated by recent inelastic neutron scattering experiments up to a high-energy region for La-based cuprates, we compute (\mathbf{q}, ω) maps of the imaginary part of the dynamical magnetic susceptibility $\chi(\mathbf{q}, \omega)$ in the slave-boson mean-field approximation to the two-dimensional t - J model. While the strong spectral weight appears at incommensurate positions, namely at $\mathbf{q} \neq \mathbf{Q} \equiv (\pi, \pi)$, for low energy, the incommensurate signals disperse with increasing ω and finally merge into a commensurate signal at a particular energy $\omega = \omega_{\mathbf{Q}}$. These features are seen in both the d -wave pairing state and the normal state. In particular, the incommensurate signals below $\omega_{\mathbf{Q}}$ in the normal state are due to the Fermi surface geometry, which we expect for La-based cuprates because of a tendency to d -wave type Fermi surface deformations. Above $\omega_{\mathbf{Q}}$, strong signals appear to trace an upward dispersion especially for a low doping rate in the d -wave pairing state while typically broad spectral weight is obtained around $\mathbf{q} = \mathbf{Q}$ in the normal state. Salient features of magnetic excitations in La-based cuprates are thus naturally captured in terms of particle-hole excitations. Global understanding of magnetic excitations in high- T_c cuprates is discussed through a comparison with magnetic excitations in $\text{YBa}_2\text{Cu}_3\text{O}_y$.

PACS numbers: 74.25.Ha, 74.72.Dn, 74.20.Mn, 71.10.Fd

I. INTRODUCTION

A major theoretical issue to understand the physics of high-temperature superconductors concerns their magnetic excitations. Most of inelastic neutron scattering measurements were performed for two high- T_c cuprates, $\text{La}_{2-x}\text{Sr}_x\text{CuO}_4$ (LSCO) and $\text{YBa}_2\text{Cu}_3\text{O}_y$ (YBCO). For low temperature and low energy, incommensurate (IC) magnetic peaks are realized in both LSCO[1, 2] and YBCO[3, 4, 5], that is, the peaks of the imaginary part of the dynamical magnetic susceptibility $\chi(\mathbf{q}, \omega)$ appear at $\mathbf{q} = (\pi, \pi \pm 2\pi\eta)$ and $(\pi \pm 2\pi\eta, \pi)$; η parametrizes the degree of incommensurability. Above the superconducting transition temperature T_c or possibly above the pseudogap temperature T^* , the IC peaks merge into a commensurate peak in YBCO[3, 5, 6] while LSCO still retains IC signals up to a temperature much higher than T_c . [1, 7, 8, 9]

The size of the incommensurability η depends on the excitation energy ω . For YBCO, η decreases with increasing ω and vanishes at a specific energy $\omega_{\mathbf{Q}}^{\text{res}}$. This commensurate signal was called a “resonance peak”, [10, 11, 12, 13] which is now regarded to be continuously connected with the IC signals observed for lower energy, that is the peak disperses smoothly downwards to lower energy when \mathbf{q} is shifted away from \mathbf{Q} . [5, 6, 14, 15] Above the resonance energy, on the other hand, peaks of magnetic excitations trace an upward dispersion. [5, 16] For LSCO, the energy dependence of η was relatively weak compared to YBCO [17] and such a robustness of the IC signals was often contrasted with the behavior in YBCO. However, recent high energy neutron scattering data for LSCO with $x = 0.10$ and 0.16 , [18] and $\text{La}_{2-x}\text{Ba}_x\text{CuO}_4$ (LBCO) with $x = 0.125$ [19] revealed that the IC peaks disperse with ω . In particular, it was found in LBCO that the IC peaks merge into a commensurate peak around 55 meV, [19] above which upward dispersive features appear, similar to YBCO except that the data for YBCO were obtained below T_c while those for LBCO above T_c .

Magnetic excitations in La-based cuprates are often interpreted in terms of the spin-charge stripe scenario, [20] according to which (a tendency to) charge stripe ordering plays a central role. This scenario is based on the observation of two charge order satellite signals at both $\mathbf{q} = (0, \pm 4\pi\eta)$ and $(\pm 4\pi\eta, 0)$, whose wavevectors are just twice as large as those of the magnetic IC signals, in Nd-doped LSCO with $x = 0.10$, [21] 0.12 , [20, 22] and 0.15 , [23] $\text{La}_{2-x}\text{Ba}_x\text{CuO}_4$ (LBCO) with $x = 0.125$, [9] and Sr-doped LBCO with the hole density 0.125 . [24, 25] It is assumed that each CuO_2 plane has charge stripes characterized by a

single wavevector $\mathbf{q} = (0, \pm 4\pi\eta)$ or $(\pm 4\pi\eta, 0)$. Hence the observed two charge order signals are speculated to be superposition originating from different CuO_2 planes. Although such charge order signals were very weak and were observed neither for other doping rates nor in other cuprate superconductors such as YBCO and LSCO, the stripe scenario has attracted much interest.[26]

There is another scenario based on conventional particle-hole excitations around the Fermi surface (FS), often referred to as the fermiology scenario.[27, 28, 29, 30, 31] This scenario was explored in more detail and turned out to capture many important features of magnetic excitations in both YBCO[32, 33, 34, 35, 36, 37, 38, 39, 40, 41, 42, 43, 44] and LSCO.[35, 37, 45] In particular, to be reconciled with a Fermi surface shape implied by angle-resolved photoemission spectroscopy (ARPES),[46, 47] the fermiology scenario for LSCO was extended by invoking the idea of a d -wave type Fermi surface deformation (d FSD),[48] which is frequently called d -wave Pomeranchuk instability:[49] the FS expands along the k_x direction and shrinks along the k_y direction, or vice versa. Comprehensive calculations of magnetic excitations for this d -wave-deformed FS[45] showed that prominent features of magnetic excitations in LSCO are well-captured within the fermiology scenario. However, these calculations were confined to a low energy region of magnetic excitations. It is interesting to see whether the fermiology scenario can capture recently reported data for a high energy region in La-based cuprates also,[19] since such data were often discussed within spin-charge stripe scenarios.[50, 51, 52]

In this paper, we extend a previous calculation in Ref.[45], which was intended for magnetic excitations in the low energy region for LSCO, to the high energy region. We compute the dynamical magnetic susceptibility $\chi(\mathbf{q}, \omega)$ in the slave-boson mean-field scheme of the two-dimensional (2D) t - J model. Combining the idea of the d FSD with magnetic excitations, we show that salient features of magnetic excitations in La-based cuprates are well-captured up to high energy in terms of particle-hole excitations. We discuss how similarities and differences of magnetic excitations between LSCO and YBCO arise in the present theory.

The paper is structured as follows. In Sec. II, we present the slave-boson mean-field scheme of the t - J model and show how the d FSD is obtained in this scheme. The dynamical magnetic susceptibility $\chi(\mathbf{q}, \omega)$ is formulated in the RPA with a renormalization factor.[34, 53] In Sec. III, numerical results of (\mathbf{q}, ω) maps of $\text{Im}\chi(\mathbf{q}, \omega)$ are presented up to high energy for several choices of temperature T and hole density. In Sec. IV, we compare our results

with neutron scattering data in La-based cuprates and discuss similarities and differences of magnetic excitations between La-based cuprates and YBCO from the present theoretical viewpoint. Sec. V is a conclusion.

II. MODEL AND FORMALISM

We take the 2D t - J model on a square lattice

$$H = - \sum_{\mathbf{r}, \mathbf{r}', \sigma} t^{(l)} \tilde{c}_{\mathbf{r}\sigma}^\dagger \tilde{c}_{\mathbf{r}'\sigma} + J \sum_{\langle \mathbf{r}, \mathbf{r}' \rangle} \mathbf{S}_{\mathbf{r}} \cdot \mathbf{S}_{\mathbf{r}'} \quad (1)$$

defined in the Fock space with no doubly occupied sites. The operator $\tilde{c}_{\mathbf{r}\sigma}^\dagger$ ($\tilde{c}_{\mathbf{r}\sigma}$) creates (annihilates) an electron with spin σ on site \mathbf{r} , while $\mathbf{S}_{\mathbf{r}}$ is the spin operator. $J(> 0)$ is a superexchange coupling between the nearest neighbor sites. We take into account hopping amplitudes $t^{(l)}$ up to the l th nearest neighbors ($l \leq 3$), which are denoted by the conventional notation, t , t' , and t'' , respectively.

We introduce the slave particles, $f_{\mathbf{r}\sigma}$ and $b_{\mathbf{r}}$, as $\tilde{c}_{\mathbf{r}\sigma} = b_{\mathbf{r}}^\dagger f_{\mathbf{r}\sigma}$, where $f_{\mathbf{r}\sigma}$ ($b_{\mathbf{r}}$) is a fermion (boson) operator that carries spin σ (charge e), and $\mathbf{S}_{\mathbf{r}} = \frac{1}{2} f_{\mathbf{r}\alpha}^\dagger \boldsymbol{\sigma}_{\alpha\beta} f_{\mathbf{r}\beta}$ with the Pauli matrices $\boldsymbol{\sigma} = (\sigma^x, \sigma^y, \sigma^z)$. The slave bosons and fermions are linked by the local constraint $b_{\mathbf{r}}^\dagger b_{\mathbf{r}} + \sum_{\sigma} f_{\mathbf{r}\sigma}^\dagger f_{\mathbf{r}\sigma} = 1$. This is an exact transformation known as the slave-boson formalism. We then decouple the interaction with the so-called resonating-valence-bond (RVB) mean fields:[54] $\chi_{\tau} \equiv \langle \sum_{\sigma} f_{\mathbf{r}\sigma}^\dagger f_{\mathbf{r}'\sigma} \rangle$, $\langle b_{\mathbf{r}}^\dagger b_{\mathbf{r}'} \rangle$, and $\Delta_{\tau} \equiv \langle f_{\mathbf{r}\uparrow} f_{\mathbf{r}'\downarrow} - f_{\mathbf{r}\downarrow} f_{\mathbf{r}'\uparrow} \rangle$, with $\boldsymbol{\tau} = \mathbf{r}' - \mathbf{r}$. These mean fields are assumed to be real constants independent of sites \mathbf{r} . We approximate the bosons to condense at the bottom of the band, which leads to $\langle b_{\mathbf{r}}^\dagger b_{\mathbf{r}'} \rangle = \delta$, where δ is the hole density. The resulting Hamiltonian reads

$$H_0 = \sum_{\mathbf{k}} \begin{pmatrix} f_{\mathbf{k}\uparrow}^\dagger & f_{-\mathbf{k}\downarrow} \end{pmatrix} \begin{pmatrix} \xi_{\mathbf{k}} & -\Delta_{\mathbf{k}} \\ -\Delta_{\mathbf{k}} & -\xi_{\mathbf{k}} \end{pmatrix} \begin{pmatrix} f_{\mathbf{k}\uparrow} \\ f_{-\mathbf{k}\downarrow}^\dagger \end{pmatrix} \quad (2)$$

with a global constraint $\sum_{\sigma} \langle f_{\mathbf{r}\sigma}^\dagger f_{\mathbf{r}\sigma} \rangle = 1 - \delta$; the \mathbf{k} summation is over $|k_{x(y)}| \leq \pi$. The RVB mean fields enter in $\xi_{\mathbf{k}}$ and $\Delta_{\mathbf{k}}$, and are determined by minimizing the free energy. We obtain $\chi_x = \chi_y = \chi$ and $\Delta_x = -\Delta_y = \Delta$ (d -wave paring). The explicit momentum dependence of the dispersion is given by

$$\begin{aligned} \xi_{\mathbf{k}} &= -2 [\bar{t}_x \cos k_x + \bar{t}_y \cos k_y \\ &+ 2t' \delta \cos k_x \cos k_y + t'' \delta (\cos 2k_x + \cos 2k_y)] - \mu, \end{aligned} \quad (3)$$

where $\bar{t}_x = \bar{t}_y = \bar{t} = t\delta + \frac{3}{8}J\chi$ and μ is the chemical potential, and the gap function is given by

$$\Delta_{\mathbf{k}} = -\frac{3}{4}J\Delta(\cos k_x - \cos k_y). \quad (4)$$

The material dependence of high- T_c cuprates is taken into account mainly by different choices of band parameters.[27, 29, 55, 56, 57] Following previous work for La-based cuprates,[29, 45] we choose $t/J = 4$, $t'/t = -1/6$, and $t''/t = 0$. In the course of the present work, we noticed that incommensurate structures of $\text{Im}\chi(\mathbf{q}, \omega)$ in the normal state become clearer for a larger t/J , showing better agreement with neutron scattering data. Note that the present choice of t/J is consistent with an *ab initio* calculation[58], which showed that realistic values for t/J lie in the range 2 – 5.

The obtained FS is electronlike (holelike) for $\delta \gtrsim 0.10$ ($\delta \lesssim 0.10$) [Fig. 1(a)]. This FS seems to be inconsistent with ARPES data where a holelike FS was implied in a much wider hole-doping region ($\delta \lesssim 0.20$);[46] the reported FS looked nearly the same as a FS in YBCO.[59] If this were the case, a fermiology scenario predicts that magnetic excitations in LSCO should be essentially the same as those in YBCO, which contradicts with neutron scattering data especially for the normal state. This problem was considered in the 2D t - J model. It was found that the system has a tendency to a d -wave type Fermi surface symmetry breaking.[48] The same tendency was also found in the Hubbard model.[60] This d FSD tendency is generated by forward scattering interactions of electrons close to the FS around $(\pi, 0)$ and $(0, \pi)$, and may be a generic feature as seen in various works: the slave-boson mean-field theory,[48, 61] the exact diagonalization analysis,[62] and the variational Monte Carlo study[63] of the t - J model, various renormalization group studies[60, 64, 65] and the renormalized perturbation theory[66] of the Hubbard model, and the mean-field theory of the extended Hubbard model.[67]

The d FSD competes with d -wave superconductivity.[48, 60, 61, 63, 64, 65, 66] In the t - J model,[48, 61, 63] the d -wave pairing instability is dominant and the spontaneous d FSD does not happen. However, the system still retains appreciable correlations of the d FSD,[48, 61, 62, 63] which make the system very sensitive to a small external anisotropy, leading to a strongly deformed FS. A natural origin of this anisotropy lies in crystal structures. La-based cuprates have the low-temperature tetragonal lattice (LTT) structure.[68, 69, 70] It yields a small xy anisotropy, the direction of which alternates along the z -axis. Through a coupling to the LTT, therefore, we can expect an alternate stacking of a strongly deformed FS as

shown in Fig. 2. Because of a weak interlayer coupling, the resulting Fermi surfaces have two sheets, an inner electronlike FS and an outer holelike FS. The FS reported by Ino *et al.*[46] may correspond to the outer holelike FS; the inner electronlike FS has not been detected successfully by ARPES.

Although the deformed FS can be determined in a self-consistent calculation,[44, 48] we here deform a FS by hand by introducing a parameter α

$$\bar{t}_{x(y)} = \alpha \bar{t} \quad (5)$$

with keeping $\bar{t}_{y(x)} = \bar{t}$. For simplicity we do not consider an interlayer coupling and compute magnetic excitations for the superimposed FSs shown in Fig. 1(b). We first determine RVB mean fields self-consistently for $\alpha = 1$, and then tune α to get a FS compatible with ARPES;[46] we choose $\alpha = 0.85$ for $\delta = 0.15$ [Fig. 1(b)]. Since we here tune α by hand, the resulting hole density slightly deviates from $\delta = 0.15$ to be 0.156.

We investigate magnetic excitations for both FSs shown in Figs. 1(a) and (b). The irreducible dynamical magnetic susceptibility $\chi_0(\mathbf{q}, \omega)$ is given by

$$\begin{aligned} \chi_0(\mathbf{q}, \omega) = & \frac{1}{4N} \sum_{\mathbf{k}} \left[C_{\mathbf{k}, \mathbf{k}+\mathbf{q}}^+ \left(\tanh \frac{E_{\mathbf{k}}}{2T} - \tanh \frac{E_{\mathbf{k}+\mathbf{q}}}{2T} \right) \frac{1}{E_{\mathbf{k}} - E_{\mathbf{k}+\mathbf{q}} + \omega + i\Gamma} \right. \\ & + \frac{1}{2} C_{\mathbf{k}, \mathbf{k}+\mathbf{q}}^- \left(\tanh \frac{E_{\mathbf{k}}}{2T} + \tanh \frac{E_{\mathbf{k}+\mathbf{q}}}{2T} \right) \\ & \left. \times \left(\frac{1}{E_{\mathbf{k}} + E_{\mathbf{k}+\mathbf{q}} + \omega + i\Gamma} + \frac{1}{E_{\mathbf{k}} + E_{\mathbf{k}+\mathbf{q}} - \omega - i\Gamma} \right) \right], \quad (6) \end{aligned}$$

where $E_{\mathbf{k}} = \sqrt{\xi_{\mathbf{k}}^2 + \Delta_{\mathbf{k}}^2}$, Γ is a positive infinitesimal, and

$$C_{\mathbf{k}, \mathbf{k}+\mathbf{q}}^{\pm} = \frac{1}{2} \left(1 \pm \frac{\xi_{\mathbf{k}} \xi_{\mathbf{k}+\mathbf{q}} + \Delta_{\mathbf{k}} \Delta_{\mathbf{k}+\mathbf{q}}}{E_{\mathbf{k}} E_{\mathbf{k}+\mathbf{q}}} \right). \quad (7)$$

In a renormalized random phase approximation (RPA)[34, 53] the dynamical magnetic susceptibility $\chi(\mathbf{q}, \omega)$ is given by

$$\chi(\mathbf{q}, \omega) = \frac{\chi_0(\mathbf{q}, \omega)}{1 + J(\mathbf{q})\chi_0(\mathbf{q}, \omega)}, \quad (8)$$

where

$$J(\mathbf{q}) = 2rJ(\cos q_x + \cos q_y) \quad (9)$$

with a renormalization factor r . In the plain RPA one has $r = 1$, which leads to a divergence of $\chi(\mathbf{q}, 0)$ around $\mathbf{q} \sim (\pi, \pi)$ in a wide hole-doping region ($\delta \lesssim 0.17$) in the d -wave pairing

state, signaling an instability to the antiferromagnetic (AF) state. However, fluctuations not included in the RPA obviously suppress the AF instability as shown in several numerical studies.[71, 72, 73] This aspect may be roughly taken into account in a phenomenological way by setting $r < 1$. [34, 53] Here we choose $r = 0.35$, which confines the AF instability to $\delta \lesssim 0.02$, consistent with the phase diagram of LSCO.[74]

III. RESULTS

We compute $\chi(\mathbf{q}, \omega)$ numerically for the FS shown in Fig. 1(a) and then for that shown in Fig. 1(b). A positive infinitesimal Γ in Eq. (6) is replaced by $\Gamma = 0.01J$ in the d -wave pairing state and $\Gamma = 0.05J$ in the normal state. Although the choice of a finite Γ is done for numerical convenience, it may simulate damping of quasiparticles by static defects in real materials and broadening due to limited energy resolution in inelastic neutron scattering experiments.

Figure 3 shows (\mathbf{q}, ω) maps of the imaginary part of $\chi(\mathbf{q}, \omega)$ for the FS shown in Fig. 1(a) for several choices of temperatures; \mathbf{q} is scanned along $(0.4\pi, \pi) \leq \mathbf{q} \leq (\pi, \pi)$ and $(\pi, \pi) \geq \mathbf{q} \geq (0.5\pi, 0.5\pi)$; along each direction the highest weight positions of $\text{Im}\chi(\mathbf{q}, \omega)$ are represented by cross symbols; in Fig. 3(a) we also plot the threshold energy of individual particle-hole excitations by a gray line; Figures 3(a) and (b) are composed of three different energy regions with an optimal color map scale. There appear gapless excitations along $\mathbf{q} = (q, q)/\sqrt{2}$ in Fig. 3(a). This diagonal IC signal is due to scattering processes between gap nodes of the d -wave singlet pairing, as already clarified about a decade ago.[28, 30] With increasing ω , scattering processes around IC positions at $\mathbf{q} = (\pi \pm 2\pi\eta, \pi)$ and $(\pi, \pi \pm 2\pi\eta)$ begin to contribute. The highest spectral weight positions (cross symbols) appear close to the threshold energy for both the IC and the diagonal IC signals; the IC signal becomes stronger than the diagonal IC signal. The incommensurability η typically tends to decrease with ω , resulting in a commensurate peak at a particular energy ($\omega \approx 0.45J$), which we define as $\omega_{\mathbf{Q}}$; note that $\omega_{\mathbf{Q}}$ corresponds also to a peak energy of $\text{Im}\chi(\mathbf{Q}, \omega)$ in the d -wave pairing state. Looking closely at a region near $\omega_{\mathbf{Q}}$, we find that the peak position of $\text{Im}\chi(\mathbf{q}, \omega)$ is located slightly below the threshold energy, where the denominator in Eq. (8) vanishes, that is, $\text{Im}\chi(\mathbf{q}, \omega)$ has a pole. Hence the strong signals near $\omega \approx \omega_{\mathbf{Q}}$ are interpreted as collective particle-hole excitations, namely the so-called resonance. But the peak position appears

very close to the threshold energy, not well inside the gap. Thermal broadening and the spectral weight broadening due to a finite Γ [Eq. (6)] easily make the resonance overdamped through mixing with individual particle-hole excitations. In addition, the (\mathbf{q}, ω) region where the resonance is realized is very limited. Therefore, particle-hole excitations below $\omega_{\mathbf{Q}}$ are mainly characterized by a downward dispersion of individual excitations, which traces the \mathbf{q} dependent threshold energy.

Above $\omega_{\mathbf{Q}}$, the strong spectral weight appears around $\mathbf{q} = \mathbf{Q}$ (cross symbols). We can, however, read off from Fig. 3(a) that such a commensurate signal is accompanied by IC and diagonal IC substructures for $\omega \gtrsim 0.5J$, which disperse outwards with increasing ω .

The (\mathbf{q}, ω) map in Fig. 3(a) is robust against temperature as seen in Fig. 3(b) and the downward dispersion below $\omega_{\mathbf{Q}}$ remains even in the normal state, namely above $T_{\text{RVB}} (= 0.104J)$ [Fig. 3(c)]; T_{RVB} is the onset temperature of the d -wave pairing gap, and is interpreted as the pseudogap crossover temperature T^* in the underdoped regime and as the superconducting phase transition temperature T_c in the overdoped regime of high- T_c cuprates.[54] Although IC and diagonal IC peaks are seen in Fig. 3(c), the peak structures are very broad because of thermal broadening. When temperature is reduced under the condition $\Delta \equiv 0$ (χ_τ and μ are determined self-consistently), we see clearer IC and diagonal IC signals in Fig. 3(d); the former is stronger than the latter. These incommensurate structures in the normal state can be traced back to the FS geometry shown in Fig. 1(a). Besides the presence of incommensurate nesting vectors, there are no particle-hole scattering processes across the FS with $\mathbf{q} = \mathbf{Q}$ and a small ω , which substantially reduces the spectral weight around \mathbf{Q} , leading to robust incommensurate structures of magnetic excitations. In Figs. 3(c) and (d), we see a IC substructure above $\omega \sim 0.2J$ along $\mathbf{q} = (q_x, \pi)$, which disperses outwards with increasing ω . This substructure becomes stronger for a larger δ and a smaller Γ .

Next we analyze the δ dependence of $\text{Im}\chi(\mathbf{q}, \omega)$. Figure 4 shows (\mathbf{q}, ω) maps of $\text{Im}\chi(\mathbf{q}, \omega)$ in the d -wave pairing state ($T = 0.01J$). A downward dispersive feature below $\omega_{\mathbf{Q}}$ still appears for a lower δ , accompanied by a reduction of $\omega_{\mathbf{Q}}$. Above $\omega_{\mathbf{Q}}$, on the other hand, an upward dispersive feature shows up with decreasing δ . In particular, its spectral weight becomes larger than that of the downward dispersion in Fig. 4(b) (see values of color map index). This upward dispersion is not due to collective excitations, but just a peak of individual particle-hole excitations. In the vicinity of the AF instability ($\delta \approx 0.02$), however,

this upward dispersion changes into an overdamped collective mode in the sense that the real part of the denominator of Eq. (8) vanishes. In the normal state, low-energy incommensurate structures become less clear for a lower δ since the FS geometry tends to allow particle-hole scattering processes with $\mathbf{q} = \mathbf{Q}$ on the FS.

Results similar to Figs. 3 and 4 are obtained for the FS shown in Fig. 1(b). (\mathbf{q}, ω) maps of $\text{Im}\chi(\mathbf{q}, \omega)$ are shown in Fig. 5 for several choices of T . In Fig. 5(a), peak positions of $\text{Im}\chi(\mathbf{q}, \omega)$ (cross symbols) trace a downward dispersion below $\omega_{\mathbf{Q}} (= 0.49J)$, which comes from individual particle-hole excitations. While a collective mode, namely the resonance, does not appear in Fig. 5(a) ($\delta = 0.15$), it can appear for a lower doping region. But even in this case, we checked that the collective mode is not well separated from the continuum excitations and thus easily overdamped for a finite T and Γ . Moreover the collective mode appears in a very limited (\mathbf{q}, ω) region as seen in Fig. 3(a). In this sense, the downward dispersion below $\omega_{\mathbf{Q}}$ is characterized mainly by individual excitations even for a lower doping rate. Although spectral weight above $\omega_{\mathbf{Q}}$ is characterized by a commensurate signal at $\mathbf{q} = \mathbf{Q}$, we see a small segment of an upward dispersion just above $\omega_{\mathbf{Q}}$ in Fig. 5(a). When the hole density is decreased, this upward dispersion becomes clearer and a result similar to Fig. 4 is obtained. Overall features seen in Fig. 5(a) still survive for a higher temperature [Fig. 5(b)], although the temperature in Fig. 5(b) is high enough to smear the segment of an upward dispersion for $\omega \gtrsim \omega_{\mathbf{Q}}$. Even above $T_{\text{RVB}} (= 0.104J)$, incommensurate structures are still seen in Fig. 5(c) and become clearer when temperature is reduced under the condition of $\Delta \equiv 0$ [Fig. 5(d)]. The robust property of the incommensurate structures in the normal state [Figs. 5(c) and (d)] can be understood in terms of the geometry of each deformed FS shown in Fig. 1(b) by the same argument as that already given in the context of Fig. 3. In reality, there is a weak interlayer coupling and thus the resulting FSs are composed of a holelike FS and an electronlike FS as shown in Fig. 2, which then allows low-energy scattering processes with $\mathbf{q} = \mathbf{Q}$ through the interlayer coupling. Such effects are, however, too weak to smear incommensurate structures for a realistic parameter as was explicitly calculated in Ref. [45].

IV. DISCUSSION

A. Magnetic excitations in La-based cuprates

Now we compare our results with neutron scattering data. For both FSs shown in Figs. 1(a) and (b), we have obtained IC magnetic excitations for a relatively low ω not only in the d -wave pairing state but also in the normal state [Figs. 3 and 5], which well captures the most prominent feature of magnetic excitations in La-based cuprates.[1, 7, 8, 9]

The incommensurability typically decreases with increasing ω and the signals finally merge into a commensurate peak at $\omega = \omega_{\mathbf{Q}}$. This dispersive feature is consistent with recent data for LBCO with $x = 0.125$,[19] and also for LSCO with $x = 0.10$ and 0.16 [18] where measurements were performed up to a certain energy below $\omega_{\mathbf{Q}}$.

For a higher energy region in LBCO with $x = 0.125$, Tranquada *et al.*[19] reported upward dispersive signals of $\text{Im}\chi(\mathbf{q}, \omega)$. Their obtained spectral weight distribution was very broad with substantial spectral weight at $\mathbf{q} = \mathbf{Q}$, and the intensity difference between IC (or diagonal IC) positions and a commensurate position was very small. Our results for $\delta = 0.15$ (Figs. 3 and 5) show typically a broad spectral weight around $\mathbf{q} = \mathbf{Q}$ for a high energy region, but an upward dispersive feature shows up with decreasing δ in the d -wave pairing state (Fig. 4). Although their measurement[19] was performed above T_c , we may assume the data were obtained in the pseudogap state in LBCO, which is associated with the d -wave pairing state in the slave-boson mean-field theory.[54] Under this assumption, we can capture their data within the present study.

Because of d FSD correlations, the shape of the FS in La-based cuprates may depend strongly on the crystal structure.[48] In the presence of the LTT structure, which was observed in LBCO[68], Nd-doped LSCO[69], and LSCO with $x = 0.12$ [70], we expect that d FSD correlations lead to a strongly deformed FS as shown in Fig. 2 through coupling to a small xy anisotropy of the lattice. The corresponding magnetic excitations are shown in Fig. 5. Even in the absence of the (static) LTT, the soft phonon mode toward the LTT structural phase transition, whose energy ω_{ph} is about a few meV, was observed in LSCO with $x \lesssim 0.18$ [75, 76, 77, 78] and LBCO with $x = 0.125$ [79]. In this case we expect dynamical fluctuations of the d FSD within a time scale shorter than ω_{ph}^{-1} . Thus high energy probes such as ARPES and neutron scattering may see an instantaneous d FSD. On the

other hand, in the absence of the LTT and its slow fluctuations, which we expect roughly for $T \gtrsim 100 - 200\text{K}$, [75, 76, 77, 78, 79] no driving force leading to a strongly deformed FS may be present. We expect a FS as in Fig. 1 (a) and magnetic excitations as in Figs. 3 and 4. In the present $d\text{FSD}$ correlation scenario, therefore, the change of the FS shape is predicted as function of T . The ARPES data for high T have not yet been obtained for La-based cuprates and this prediction can be tested in a future.

An indirect evidence of the FS change was recently obtained in a neutron scattering experiment for LBCO with $x = 0.125$. This material shows almost a first-order-like LTT structural phase transition at 60K. [79] Fujita *et al.* [9] measured a temperature dependence of the incommensurability η at a low energy and found a sizable change of η at the LTT transition. This is naturally understood in terms of the (static) FS change scenario from Fig. 1(a) to Fig. 1(b) below 60K; the FS shown in Fig. 1(b) tends to favor a larger η , the same tendency as the experiment. The authors in Ref. [9], however, interpreted the data differently as a lock-in effect that the periodicity of charge stripes tends to be commensurate with the lattice potential of the LTT structure, although a charge order signal developed gradually below 50K, not directly below the LTT transition temperature.

The state with a d -wave deformed FS has the same symmetry as the so-called electronic nematic state. [80] The nematic order was extensively discussed for cuprates. [26] However this nematic order was discussed as coming from partial spin-charge stripe order, not from $d\text{FSD}$ correlations; magnetic excitations were then discussed in terms of stripes. Our $d\text{FSD}$ does not require charge stripes nor their fluctuations, but is driven by forward scattering processes of quasiparticles, which provides another route to the nematic state. An interesting open question is whether the $d\text{FSD}$ state might have an instability toward a charge ordered state such as stripes. Even if it were the case, our calculation shows that many prominent features of magnetic excitations observed in La-based cuprates are already well-captured without stripes. Observations of weak charge order signals [9, 20, 21, 22, 23, 24, 25] do not necessarily mean that charge stripes are crucial to magnetic excitations. Effects of a charge order on magnetic excitations can be higher order corrections beyond the present renormalized RPA and might be responsible for a realization of static IC antiferromagnetic order around hole density $1/8$ in La-based cuprates, [9, 20, 21, 24, 81, 82] which cannot be captured in the present framework.

B. Comparison with magnetic excitations in YBCO

We finally discuss how similarities and differences of magnetic excitations between La-based cuprates and YBCO arise from the present framework. In the slave-boson mean-field theory, material dependences are described by different choices of band parameters. For La-based cuprates, we have taken $t/J = 4$, $t'/t = -1/6$, $t''/t = 0$, and $r = 0.35$ (see Sec. II) while $t/J = 2.5$, $t'/t = -0.30$, $t''/t = 0.15$, and $r = 0.5$ were invoked for YBCO (see Ref. [44], where the bilayer coupling was also taken into account and a comprehensive study of magnetic excitations in YBCO was performed including effects of the d FSD).

A well-known distinction between La-based cuprates and YBCO is that low-energy IC magnetic signals are realized up to a temperature much higher than T_c in the former,[1, 7, 8, 9] while they are realized only below T_c or possibly below the pseudogap temperature T^* in the latter.[3, 5, 6] This difference comes from a FS difference due to different choices of t'/t and t''/t . For the FS shown in Fig. 1, there are no particle-hole scattering processes with $\mathbf{q} = \mathbf{Q}$ for low energy, yielding robust incommensurate structures even in the normal state, while the FS for YBCO[59] allows such scattering processes, smearing incommensurate features in the normal state. We confirm early works[27, 28, 29, 30] to understand this material dependence of magnetic excitations.

In the d -wave superconducting state, on the other hand, both LSCO[2, 18] and YBCO[5, 6, 14, 15] show IC magnetic signals for low ω and its incommensurability η decreases with increasing ω . This behavior is well-reproduced in the present framework, and does not depend on the choice of band parameters as emphasized before.[35]

The so-called resonance signals of magnetic excitations were reported for YBCO in the superconducting state[10, 11, 12] and a pseudogap state[13], but not for LSCO. In the present theory, this resonance is interpreted as collective particle-hole excitation as already discussed by many authors.[31, 32, 33, 34, 35, 36, 37, 38, 39, 40, 41, 42, 43, 44] The realization of collective excitations depends strongly on the choice of r in Eq. (9); it is more favorable for a larger r . Although our relatively small r for LSCO can produce a resonance, its energy appears very close to the threshold energy of continuum excitations, making the resonance easily overdamped by thermal broadening and spectral broadening due to a finite Γ [Eq. (6)]. Therefore the resonance signals are not so clear for LSCO as for YBCO. It is to be noted that if we invoke a larger r for LSCO, keeping other parameters unchanged,

well-defined resonance signals appear as in the case of the parameters for YBCO.[44] There is another factor, a FS difference, which is less effective than a factor r . Since the FS invoked for LSCO (Fig. 1) is closer to the $(\pi/2, \pi/2)$ point than that for YBCO, lowest-energy particle-hole scattering processes with $\mathbf{q} = \mathbf{Q}$ appear at $k_x = k_y$ when a large d -wave pairing gap opens on the FS. For such scattering processes, the coherence factor $C_{\mathbf{k}, \mathbf{k}+\mathbf{q}}^-$ [Eq. (7)] vanishes. Hence at zero temperature the imaginary part of $\chi_0(\mathbf{Q}, \omega)$ does not show a jump at the threshold energy, but increases continuously; the corresponding real part of $\chi_0(\mathbf{Q}, \omega)$ does not have a log-divergence there. This is the case for $\delta < 0.08$ for the present parameters for La-based cuprates. Since one of well-known mechanisms of the resonance[31, 32, 33, 34, 35, 36, 37, 38, 39, 40, 41, 42, 43, 44] is based on this log-divergence of $\text{Re}\chi_0(\mathbf{Q}, \omega)$, the resonance is further disfavored for La-based cuprates.

Above the resonance energy, the so-called upward dispersive mode was found in YBCO[14, 15, 16], which was captured in the present slave-boson mean-field framework[44] as well as other phenomenological calculations.[35, 36] A similar high energy spectrum, which was much broader than that in YBCO, was also reported for LBCO with $x = 0.125$.[19] Our results in Figs. 3,4, and 5 capture this experimental data. The realization of an upward dispersion becomes more favorable for a smaller δ , a larger r , and a smaller t/J . Since the latter two factors are not respected for the present parameters for La-based cuprates, the origin of the upward dispersion is different from that for YBCO: a peak of individual particle-hole excitations (except for the vicinity of the AF instability) for La-based cuprates and overdamped collective excitations[44] for YBCO.

V. CONCLUSION

We have computed $\text{Im}\chi(\mathbf{q}, \omega)$ up to a high energy region ($\lesssim J$) and shown that salient features of magnetic excitations in La-based cuprates are well-captured in terms of particle-hole excitations. IC magnetic signals are realized for low ω in both the d -wave pairing state and the normal state, and they disperse with increasing ω , merging into a commensurate signal at $\omega = \omega_{\mathbf{Q}}$. The resonance mode can be realized close to $\omega = \omega_{\mathbf{Q}}$, which is easily overdamped by mixing with individual particle-hole excitations for finite T and Γ . Above $\omega_{\mathbf{Q}}$, upward dispersive features of $\text{Im}\chi(\mathbf{q}, \omega)$ appear especially for a low δ in the d -wave pairing state, while typically broad spectral weight distribution is obtained around $\mathbf{q} = \mathbf{Q}$ in the

normal state. In the present theory, d FSD correlations[48, 60] have played an important role for the shape of the FS. In particular, we expect a change of a (static) FS shape across the LTT structural phase transition, which in general yields a sizable change of incommensurability. Such a change was recently observed in LBCO.[9] Combined with previous work[45] focusing on the low energy region of magnetic excitations, the present study confirms the crucial role of particle-hole excitations up to high energy for magnetic excitations in La-based cuprates.

Acknowledgments

The author is grateful to C. Bernhard, M. Fujita, and R. Zeyher for helpful discussions, and especially to W. Metzner for a critical reading the manuscript.

-
- [1] T. R. Thurston, R. J. Birgeneau, M. A. Kastner, N. W. Preyer, G. Shirane, Y. Fujii, K. Yamada, Y. Endoh, K. Kakurai, M. Matsuda, Y. Hidaka, and T. Murakami, *Phys. Rev. B* **40**, 4585 (1989).
 - [2] K. Yamada, C. H. Lee, K. Kurahashi, J. Wada, S. Wakimoto, S. Ueki, H. Kimura, Y. Endoh, S. Hosoya, G. Shirane, R. J. Birgeneau, M. Greven, M. A. Kastner, and Y. J. Kim, *Phys. Rev. B* **57**, 6165 (1998).
 - [3] P. Dai, H. A. Mook, and F. Doğan, *Phys. Rev. Lett.* **80**, 1738 (1998).
 - [4] H. A. Mook, P. Dai, S. M. Hayden, G. Aeppli, T. G. Perring, and F. Doğan, *Nature* **395**, 580 (1998).
 - [5] M. Arai, T. Nishijima, Y. Endoh, T. Egami, S. Tajima, K. Tomimoto, Y. Shiohara, M. Takahashi, A. Garrett, and S. M. Bennington, *Phys. Rev. Lett.* **83**, 608 (1999).
 - [6] P. Bourges, Y. Sidis, H. F. Fong, L. P. Regnault, J. Bossy, A. Ivanov, and B. Keimer, *Science* **288**, 1234 (2000).
 - [7] G. Aeppli, T. E. Mason, S. M. Hayden, H. A. Mook, and J. Kulda, *Science* **278**, 1432 (1997).
 - [8] M. Ito, Y. Yasui, S. Iikubo, M. Soda, M. Sato, A. Kobayashi, and K. Kakurai, *J. Phys. Soc. Jpn.* **72**, 1627 (2003).
 - [9] M. Fujita, H. Goka, K. Yamada, J. M. Tranquada, and L. P. Regnault, *Phys. Rev. B* **70**,

- 104517 (2004).
- [10] J. Rossat-Mignod, L. P. Regnault, C. Vettier, P. Bourges, P. Burlet, J. Bossy, J. Y. Henry, and G. Lapertot, *Physica C* **185-189**, 86 (1991).
- [11] P. Bourges, in *The Gap Symmetry and Fluctuations in High- T_c Superconductors*, edited by J. Bok, G. Deutscher, D. Pavuna, and S. A. Wolf (Plenum, 1998), vol. B371 of *NATO ASI Series*.
- [12] H. F. Fong, P. Bourges, Y. Sidis, L. P. Regnault, J. Bossy, A. Ivanov, D. L. Milius, I. A. Aksay, and B. Keimer, *Phys. Rev. B* **61**, 14773 (2000).
- [13] P. Dai, H. A. Mook, R. D. Hunt, and F. Doğan, *Phys. Rev. B* **63**, 54525 (2001).
- [14] D. Reznik, P. Bourges, L. Pintschovius, Y. Endoh, Y. Sidis, T. Masui, and S. Tajima, *Phys. Rev. Lett.* **93**, 207003 (2004).
- [15] S. Pailhès, Y. Sidis, P. Bourges, V. Hinkov, A. Ivanov, C. Ulrich, L. P. Regnault, and B. Keimer, *Phys. Rev. Lett.* **93**, 167001 (2004).
- [16] S. M. Hayden, H. A. Mook, P. Dai, T. G. Perring, and F. Doğan, *Nature* **429**, 531 (2004).
- [17] T. E. Mason, G. Aeppli, and H. A. Mook, *Phys. Rev. Lett.* **68**, 1414 (1992).
- [18] N. B. Christensen, D. F. McMorrow, H. M. Rønnow, B. Lake, S. M. Hayden, G. Aeppli, T. G. Perring, M. Mangkorntong, N. Nohara, and H. Takagi, *Phys. Rev. Lett.* **93**, 147002 (2004).
- [19] J. M. Tranquada, H. Woo, T. G. Perring, H. Goka, G. D. Gu, G. Xu, M. Fujita, and K. Yamada, *Nature* **429**, 534 (2004).
- [20] J. M. Tranquada, B. J. Sternlieb, J. D. Axe, Y. Nakamura, and S. Uchida, *Nature* **375**, 561 (1995).
- [21] N. Ichikawa, S. Uchida, J. M. Tranquada, T. Niemöller, P. M. Gehring, S.-H. Lee, and J. R. Schneider, *Phys. Rev. Lett.* **85**, 1738 (2000).
- [22] M. v. Zimmermann, A. Vigliante, T. Niemöller, N. Ichikawa, T. Frello, J. Madsen, P. Wochner, S. Uchida, N. H. Andersen, J. M. Tranquada, D. Gibbs, and J. R. Schneider, *Europhys. Lett.* **41**, 629 (1998).
- [23] T. Niemöller, N. Ichikawa, T. Frello, H. Hünnefeld, N. H. Andersen, S. Uchida, J. R. Schneider, and J. M. Tranquada, *Eur. Phys. J. B* **12**, 509 (1999).
- [24] M. Fujita, H. Goka, K. Yamada, and M. Matsuda, *Phys. Rev. Lett.* **88**, 167008 (2002).
- [25] H. Kimura, H. Goka, M. Fujita, Y. Noda, K. Yamada, and N. Ikeda, *Phys. Rev. B* **67**, 140503(R) (2003).

- [26] S. A. Kivelson, I. P. Bindloss, E. Fradkin, V. Oganesyan, J. M. Tranquada, A. Kapitulnik, and C. Howald, *Rev. Mod. Phys.* **75**, 1201 (2003).
- [27] Q. Si, Y. Zha, K. Levin, and J. P. Lu, *Phys. Rev. B* **47**, 9055 (1993).
- [28] Y. Zha, K. Levin, and Q. Si, *Phys. Rev. B* **47**, 9124 (1993).
- [29] T. Tanamoto, H. Kohno, and H. Fukuyama, *J. Phys. Soc. Jpn.* **62**, 717 (1993).
- [30] T. Tanamoto, H. Kohno, and H. Fukuyama, *J. Phys. Soc. Jpn.* **63**, 2739 (1994).
- [31] D. Z. Liu, Y. Zha, and K. Levin, *Phys. Rev. Lett.* **75**, 4130 (1995).
- [32] N. Bulut and D. J. Scalapino, *Phys. Rev. B* **53**, 5149 (1996).
- [33] A. J. Millis and H. Monien, *Phys. Rev. B* **54**, 16172 (1996).
- [34] J. Brinckmann and P. A. Lee, *Phys. Rev. Lett.* **82**, 2915 (1999).
- [35] Y.-J. Kao, Q. Si, and K. Levin, *Phys. Rev. B* **61**, R11898 (2000).
- [36] M. R. Norman, *Phys. Rev. B* **61**, 14 751 (2000).
- [37] D. Manske, I. Eremin, and K. H. Bennemann, *Phys. Rev. B* **63**, 54517 (2001).
- [38] A. V. Chubukov, B. Jankó, and O. Tchernyshyov, *Phys. Rev. B* **63**, 180507(R) (2001).
- [39] J. Brinckmann and P. A. Lee, *Phys. Rev. B* **65**, 014502 (2002).
- [40] F. Onufrieva and P. Pfeuty, *Phys. Rev. B* **65**, 54515 (2002).
- [41] J.-X. Li and C.-D. Gong, *Phys. Rev. B* **66**, 14506 (2002).
- [42] A. P. Schnyder, A. Bill, C. Mudry, R. Gilardi, H. M. Rønnow, and J. Mesot, *Phys. Rev. B* **70**, 214511 (2004).
- [43] I. Sega, P. Prelovšek, and J. Bonča, *Phys. Rev. B* **68**, 54524 (2003); I. Sega and P. Prelovšek, *Phys. Rev. B* **73**, 92516 (2006).
- [44] H. Yamase and W. Metzner, *Phys. Rev. B* **73**, 214517 (2006).
- [45] H. Yamase and H. Kohno, *J. Phys. Soc. Jpn.* **70**, 2733 (2001); H. Yamase, *ibid.* **71**, 1154 (2002); H. Yamase and H. Kohno, *Phys. Rev. B* **68**, 014502 (2003).
- [46] A. Ino, C. Kim, T. Mizokawa, Z.-X. Shen, A. Fujimori, M. Takaba, K. Tamasaku, H. Eisaki, and S. Uchida, *J. Phys. Soc. Jpn.* **68**, 1496 (1999); A. Ino, C. Kim, M. Nakamura, T. Yoshida, T. Mizokawa, A. Fujimori, Z.-X. Shen, T. Kakeshita, H. Eisaki, and S. Uchida, *Phys. Rev. B* **65**, 094504 (2002).
- [47] X. J. Zhou, T. Yoshida, S. A. Kellar, P. V. Bogdanov, E. D. Lu, A. Lanzara, M. Nakamura, T. Noda, T. Kakeshita, H. Eisaki, S. Uchida, A. Fujimori, Z. Hussain, and Z.-X. Shen, *Phys. Rev. Lett.* **86**, 5578 (2001).

- [48] H. Yamase and H. Kohno, J. Phys. Soc. Jpn. **69**, 332 (2000); **69**, 2151 (2000).
- [49] I. J. Pomeranchuk, Sov. Phys. JETP **8**, 361 (1958).
- [50] M. Vojta and T. Ulbricht, Phys. Rev. Lett. **93**, 127002 (2004).
- [51] G. S. Uhrig, K. P. Schmidt, and M. Grüninger, Phys. Rev. Lett. **93**, 267003 (2004).
- [52] G. Seibold and J. Lorenzana, Phys. Rev. Lett. **94**, 107006 (2005).
- [53] H. Yamase, H. Kohno, H. Fukuyama, and M. Ogata, J. Phys. Soc. Jpn. **68**, 1082 (1999).
- [54] For a review of the slave-boson mean-field theory of the two-dimensional t - J model, see H. Fukuyama, J. Phys. Chem. Solids, **59**, 447 (1998). This theory was later extended by including the possibility of a d FSD[48].
- [55] L. F. Feiner, J. H. Jefferson, and R. Raimondi, Phys. Rev. Lett. **76**, 4939 (1996).
- [56] T. Tohyama and S. Maekawa, Supercond. Sci. Technol. **13**, R17 (2000).
- [57] E. Pavarini, I. Dasgupta, T. Saha-Dasgupta, O. Jepsen, and O. K. Andersen, Phys. Rev. Lett. **87**, 47003 (2001).
- [58] M. S. Hybertsen, E. B. Stechel, M. Schluter, and D. R. Jennison, Phys. Rev. B **41**, 11068 (1990).
- [59] C. M. Schabel, C.-H. Park, A. Matsuura, Z.-X. Shen, D. A. Bonn, R. Liang, and W. N. Hardy, Phys. Rev. B **57**, 6107 (1998).
- [60] C. J. Halboth and W. Metzner, Phys. Rev. Lett. **85**, 5162 (2000).
- [61] H. Yamase, Phys. Rev. Lett. **93**, 266404 (2004).
- [62] A. Miyanaga and H. Yamase, Phys. Rev. B **73**, 174513 (2006).
- [63] B. Edegger, V. N. Muthukumar, and C. Gros, cond-mat/0609408.
- [64] I. Grote, E. Körding, and F. Wegner, J. Low Temp. Phys. **126**, 1385 (2002); V. Hankevych, I. Grote, and F. Wegner, Phys. Rev. B **66**, 094516 (2002).
- [65] C. Honerkamp, M. Salmhofer, and T. M. Rice, Eur. Phys. J. B **27**, 127 (2002).
- [66] A. Neumayr and W. Metzner, Phys. Rev. B **67**, 035112 (2003).
- [67] B. Valenzuela and M. A. H. Vozmediano, Phys. Rev. B **63**, 153103 (2001).
- [68] J. D. Axe, A. H. Moudden, D. Hohlwein, D. E. Cox, K. M. Mohanty, A. R. Moodenbaugh, and Y. Xu, Phys. Rev. Lett. **62**, 2751 (1989).
- [69] M. K. Crawford, R. L. Harlow, E. M. McCarron, W. E. Farneth, J. D. Axe, H. Chou, and Q. Huang, Phys. Rev. B **44**, 7749 (1991).
- [70] S. Sakita, F. Nakamura, T. Suzuki, and T. Fujita, J. Phys. Soc. Jpn. **68**, 2755 (1999).

- [71] G. J. Chen, R. Joynt, F. C. Zhang, and C. Gros, *Phys. Rev. B* **42**, 2662 (1990).
- [72] T. Giamarchi and C. Lhuillier, *Phys. Rev. B* **43**, 12943 (1991).
- [73] A. Himeda and M. Ogata, *Phys. Rev. B* **60**, R9935 (1999).
- [74] B. Keimer, N. Belk, R. J. Birgeneau, A. Cassanho, C. Y. Chen, M. Greven, M. A. Kastner, A. Aharony, Y. Endoh, R. W. Erwin, and G. Shirane, *Phys. Rev. B* **46**, 14034 (1992).
- [75] T. R. Thurston, R. J. Birgeneau, D. R. Gabbe, H. P. Jenssen, M. A. Kastner, P. J. Picone, N. W. Preyer, J. D. Axe, P. Böni, G. Shirane, M. Sato, K. Fukuda, and S. Shamoto, *Phys. Rev. B* **39**, 4327 (1989).
- [76] C.-H. Lee, K. Yamada, M. Arai, S. Wakimoto, S. Hosoya, and Y. Endoh, *Physics C* **257**, 264 (1996).
- [77] H. Kimura, H. Matsushita, K. Hirota, Y. Endoh, K. Yamada, G. Shirane, Y. S. Lee, M. A. Kastner, and R. J. Birgeneau, *Phys. Rev. B* **61**, 14366 (2000).
- [78] S. Wakimoto, S. Lee, P. M. Gehring, R. J. Birgeneau, and G. Shirane, *J. Phys. Soc. Jpn.* **73**, 3413 (2004).
- [79] H. Kimura, Y. Noda, H. Goka, M. Fujita, K. Yamada, and G. Shirane, *J. Phys. Soc. Jpn.* **74**, 445 (2005).
- [80] S. A. Kivelson, E. Fradkin, and V. J. Emery, *Nature* **393**, 550 (1998).
- [81] T. Suzuki, T. Goto, K. Chiba, T. Shinoda, T. Fukase, H. Kimura, K. Yamada, M. Ohashi, and Y. Yamaguchi, *Phys. Rev. B* **57**, R3229 (1998).
- [82] H. Kimura, K. Hirota, H. Matsushita, K. Yamada, Y. Endoh, S. H. Lee, C. F. Majkrzak, R. Erwin, G. Shirane, M. Greven, Y. S. Lee, M. A. Kastner, and R. J. Birgeneau, *Phys. Rev. B* **59**, 6517 (1999).

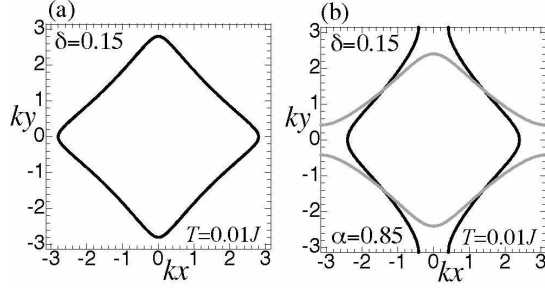


FIG. 1: Fermi surface for $\delta = 0.15$: (a) isotropic case and (b) anisotropic case with $\alpha = 0.85$, where two Fermi surfaces (solid line and gray line) are superimposed. The Fermi surface is defined by $\xi_{\mathbf{k}} = 0$ at $T = 0.01J$ in the d -wave pairing state.

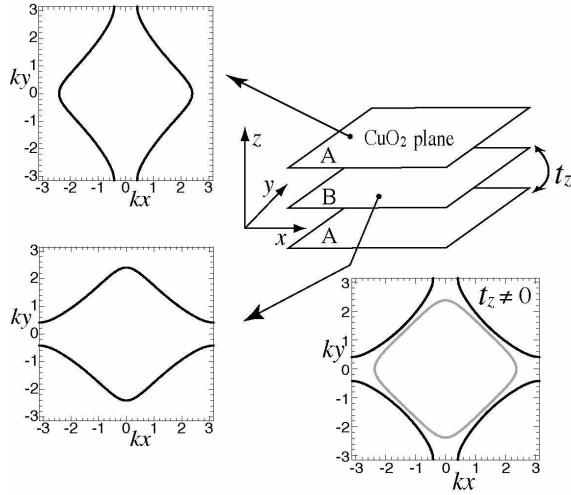


FIG. 2: Alternate stacking of d -wave deformed Fermi surfaces along the z axis in the presence of the LTT in La-based cuprates. Because of a weak interlayer coupling t_z , the resulting Fermi surfaces (right panel) are composed of a holelike Fermi surface (solid line) and an electronlike Fermi surface (gray line).

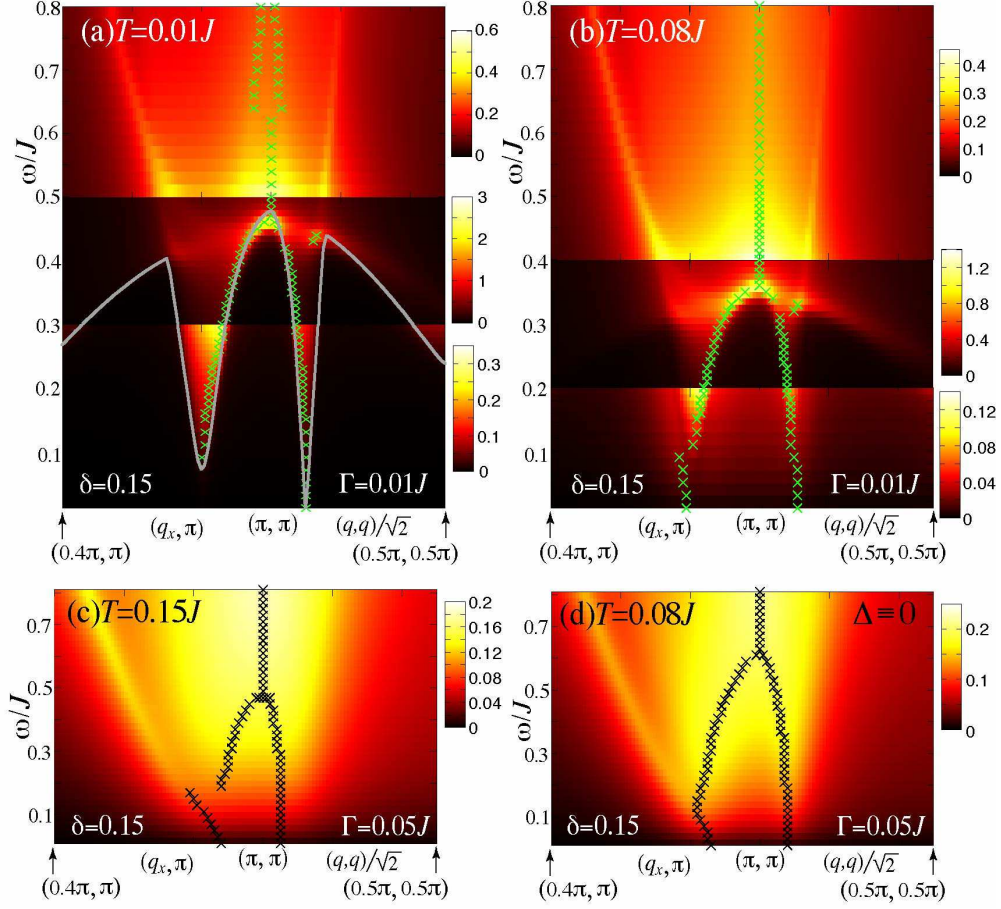


FIG. 3: (color online) (\mathbf{q}, ω) maps of $\text{Im}\chi(\mathbf{q}, \omega)$ for $\delta = 0.15$ at several choices of T for the Fermi surface shown in Fig. 1(a); $T_{RVB} = 0.104J$, but $\Delta \equiv 0$ is assumed in (d); the \mathbf{q} scan directions are $(0.4\pi, \pi) \leq \mathbf{q} \leq (\pi, \pi)$ and $(\pi, \pi) \geq \mathbf{q} \geq (0.5\pi, 0.5\pi)$; the cross symbols represent the highest weight positions along $\mathbf{q} = (q_x, \pi)$ and $(q, q)/\sqrt{2}$; the gray line in (a) is a lower edge of the continuum excitations; (a) and (b) are made of three different energy regions with an optimal color map scale.

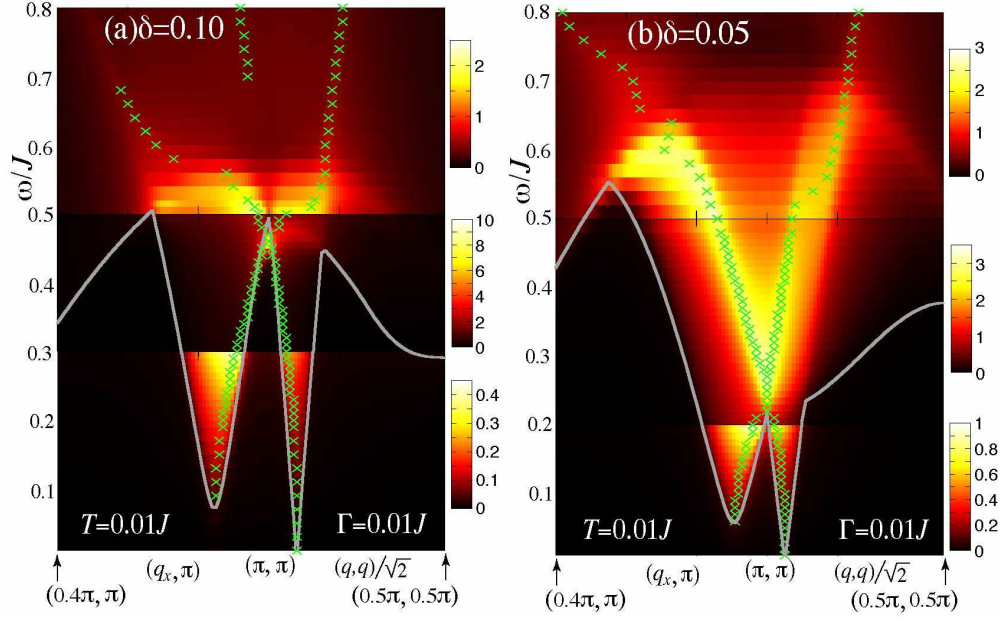


FIG. 4: (color online) (\mathbf{q}, ω) maps of $\text{Im}\chi(\mathbf{q}, \omega)$ at $T = 0.01J$ for $\delta = 0.10$ (a) and 0.05 (b); the corresponding result for $\delta = 0.15$ is shown in Fig. 3(a).

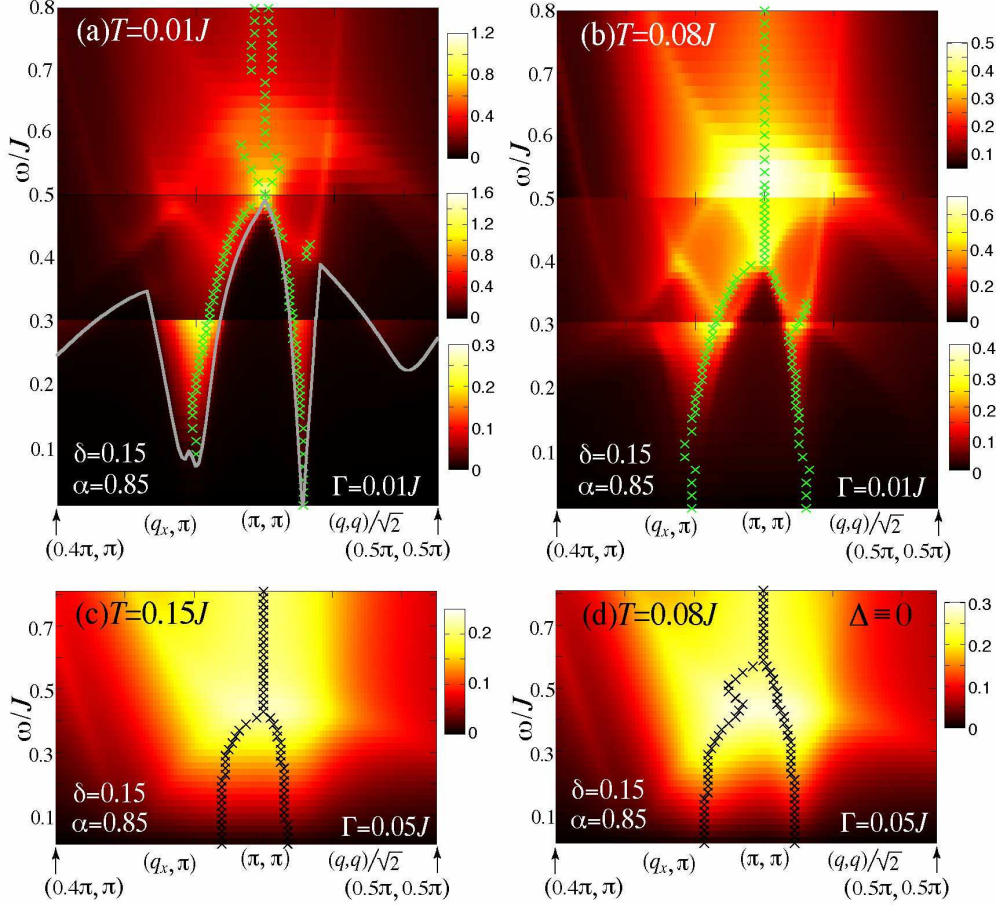


FIG. 5: (color online) (\mathbf{q}, ω) maps of $\text{Im}\chi(\mathbf{q}, \omega)$ for $\delta = 0.15$ at several choices of T for the Fermi surface shown in Fig. 1(b); $T_{RVB} = 0.104J$, but $\Delta \equiv 0$ is assumed in (d); the corresponding results for the Fermi surface in Fig. 1(a) are shown in Fig. 3.